J. Fluid Mech. (1998), *vol.* 374, *pp.* 91–116. Printed in the United Kingdom

© 1998 Cambridge University Press

Boundary layer development after a separated region

By IAN P. CASTRO[1] AND ELEANORA EPIK[2]

[1] School of Mechanical and Materials Engineering, University of Surrey, Guildford, Surrey GU2 5XH, UK

[2] Institute of Engineering Thermophysics, National Academy of Sciences of Ukraine, Kiev, Ukraine

(Received 23 June 1997 and in revised form 1 May 1998)

Measurements obtained in boundary layers developing downstream of the highly turbulent, separated flow generated at the leading edge of a blunt flat plate are presented. Two cases are considered: first, when there is only very low (wind tunnel) turbulence present in the free-stream flow and, second, when roughly isotropic, homogeneous turbulence is introduced. With conditions adjusted to ensure that the separated region was of the same length in both cases, the flow around reattachment was significantly different and subsequent differences in the development rate of the two boundary layers are identified. The paper complements, but is much more extensive than, the earlier presentation of some of the basic data (Castro & Epik 1996), confirming not only that the development process is very slow, but also that it is non-monotonic. Turbulence stress levels fall below those typical of zero-pressure-gradient boundary layers and, in many ways, the boundary layer has features similar to those found in standard boundary layers perturbed by free-stream turbulence. It is argued that, at least as far as the turbulence structure is concerned, the inner layer region develops no more quickly than does the outer flow and it is the latter which essentially determines the overall rate of development of the whole flow. Some numerical computations are used to assess the extent to which current turbulence models are adequate for such flows.

1. Introduction

There is now overwhelming evidence that the turbulence structure of classical shear flows (wakes, boundary layers, etc.) is very sensitive to the imposition of additional mean flow strain rates. Further, there is considerable evidence (both new and old) that recovery of such flows after removal of the distortion is very slow and often non-monotonic. This has been demonstrated in the context of, for example, boundary layers subjected to regions of curvature (e.g. Smits, Young & Bradshaw 1979; Alving, Smits & Watmuff 1990), mixing layers subjected to spanwise divergence and/or curvature (e.g. Castro & Bradshaw 1976; Johnson & Hancock 1989) and wakes subjected to axial pressure gradients (e.g. Narasimha & Prabhu 1972). Sometimes the distortion is such that the flow essentially changes sequentially from one kind of shear layer to another – as when, for example, a thin (maybe laminar) boundary layer separates to form an (eventually) turbulent mixing layer which bounds a recirculating flow region and then reattaches, subsequently developing into a turbulent boundary layer. Flows of this latter 'overwhelming' kind (Bradshaw & Wong 1972) are common and many authors have studied either the first transition (boundary layer to mixing layer) or the second (mixing layer to boundary layer), or both. The most widely studied

https://doi.org/10.1017/S0022112098002420 Published online by Cambridge University Press

case is that of the backward facing step (e.g. Kim, Kline & Johnston 1980; Adams & Johnston 1988) but other geometries have also been studied (see Cherry, Hillier & Latour 1984; Dyban, Epik & Yushina 1991; Ruderich & Fernholz 1986; Castro & Haque 1987 for examples).

In cases like these, less attention has generally been given to the way in which the flow eventually recovers to a standard form, although it has been clearly shown that, as in the case of the simpler distortions mentioned earlier, the recovery can be extremely slow. The early evidence accumulated by Bradshaw & Wong (1972) suggested that the outer part of the boundary layer develops much more slowly than the inner region and, more recently, other authors have emphasized this point (e.g. Jovic 1993; Jovic & Browne 1990). However, one could question whether the inner region can, in fact, ever 'recover' to its standard form while the outer flow is significantly different from that of a regular boundary layer. It is well-known that disturbances to the outer flow – like those generated by the presence of free-stream turbulence, for example – affect the inner region considerably (e.g. Hancock & Bradshaw 1989). In the case of a flow downstream of reattachment, therefore, where the outer flow certainly takes a long time to mutate from its distorted mixing layer form at reattachment to the standard boundary layer form far downstream, it could be argued that the inner region (or 'internal layer') could not possibly develop normally until the outer flow has become more normal. In view of the wide-ranging evidence of the many dynamical links between inner and outer regions of a standard boundary layer, it seems more likely that the development processes in both regions subsequent to reattachment must proceed, at least in some respects, together. Indeed, in the context of a boundary layer recovering from a region of convex curvature, Alving *et al.* (1990) argue that 'although the internal layer may be a useful concept, it seems too simplistic to describe accurately the details of the recovery process'. A recent study by Alving & Fernholz (1996) confirms this convincingly. They measured the flow throughout and downstream of a separation/reattachment region in an axisymmetric boundary layer and found that the recovery does not start at the wall and travel outwards as a growing inner layer of standard form. Rather, 'the outer layer structures survive the separation process and interfere with the regeneration of Reynolds stresses in the inner region'. In their case this continued for at least 20 boundary layer thicknesses beyond reattachment, which is about the time a normally growing inner layer would take to reach the boundary layer's outer edge (Smits & Wood 1985).

Dyban *et al.* (1991) suggested that the dominant large-eddy structures in the outer flow just downstream of reattachment and the substantial energy production there would affect the development of the inner region. They were perhaps the first to suggest some similarities between the inner region far downstream and a boundary layer affected by free-stream turbulence. Close study of the development process requires detailed turbulence data to considerable distances downstream; such data are largely non-existent. We have therefore undertaken an experimental investigation of a boundary layer developing downstream of the separated region that exists at the leading edge of a blunt, two-dimensional flat plate parallel to a free stream. Extensive turbulence measurements were made to a considerably greater downstream distance than in any previous work. Some of the basic mean flow and turbulence data have been presented in a brief, initial paper (Castro & Epik 1996) where, in particular, it was shown that the flow far downstream does indeed have features similar to those of a boundary layer beneath free-stream turbulence. For example, the turbulence stresses at about $20x_r$ downstream, where x_r is the axial length of the separated zone, are lower than those of a standard zero-pressure-gradient boundary layer at the same momentum

https://doi.org/10.1017/S0022112098002420 Published online by Cambridge University Press

thickness Reynolds number, despite the fact that just downstream of reattachment they are all very much higher. In common with turbulence recovery after some strong distortions like curvature (as mentioned earlier), the development is therefore non-monotonic. The outer region of the developing boundary layer seems to act rather like free-stream turbulence as far as the development of the inner region is concerned. We also found that the addition of genuine free-stream turbulence to this flow (with a length scale of the same order as the boundary layer thickness) seemed to have only a secondary influence on the development of the turbulence stresses. The implication is that the latter is dominated by the rate at which the 'distorted mixing layer' eddies around reattachment can be transformed to 'outer-region boundary layer' eddies. This process requires major changes in eddy structures, as suggested by Bandyopadhyay (1989), and free-stream turbulence can provide only secondary influences on it.

It should be noted that we use the term 'development', rather than 'relaxation' or 'recovery', of the flow downstream of reattachment because in this case there is no upstream turbulent boundary layer. Separation at the leading edge is fixed by the geometry, is inevitably laminar and is followed by transition in the separated shear layer before reattachment. The distortion is therefore much stronger than that studied by Alving & Fernholz (1996). The flow is also different to that, for example, downstream of the separated region behind a surface-mounted bluff obstacle immersed in a thick, turbulent boundary layer. In that case, one can more reasonably talk of the downstream flow 'relaxing' to its upstream form; if the boundary layer thickness is much greater than the body height the most serious distortions generated by the body initially occur within the inner region. There have been a number of papers which, in providing an analytical framework for considering the effects of distortions on standard flows, recognize the presence of multiple layers, each of which requires different scaling. In particular, for example, Durbin & Belcher (1992) have shown that an asymptotic analysis of adverse-pressure-gradient boundary layers requires three layers, rather than the usual two (inner and outer layers) sufficient to describe the zero-pressure-gradient boundary layer. Likewise, Counihan, Hunt & Jackson (1974) modelled the relaxing wake behind a bluff body in a deep boundary layer as a perturbation of the upstream boundary layer. Such approaches can certainly be instructive (although not always useful in practice – see Castro 1979 for discussion of the relaxing wake case). However, the present situation, as indicated earlier, constitutes development of one type of flow from an overwhelmingly perturbed version of another very different one and it is not immediately evident whether a perturbation approach would be practically very fruitful. We take the (certainly utilitarian and perhaps arguable) view that it is more appropriate to discuss the developing boundary layer in terms of the way in which the (eventual) inner and outer regions appear, given the no-slip condition, the unusual initial conditions and the possible presence of different external flows (i.e. having free-stream turbulence or not).

In this paper we therefore present a more detailed analysis of the data in order to discuss the development process more thoroughly. Some of the basic data are given again for completeness and to aid the discussion. More emphasis than before is given to the results obtained in the presence of free-stream turbulence since, by comparison with those obtained in its absence, we believe these provide significant clues to the nature of the development process. The analysis includes discussion of the cross-stream balances of turbulence kinetic energy and we have also undertaken some numerical computations of the flow using standard turbulence models. These provide further insight and, in particular, highlight some of the features of the flow which are not adequately modelled by standard methods. The experimental techniques are

https://doi.org/10.1017/S0022112098002420 Published online by Cambridge University Press

summarized in the following section, which includes a brief discussion of the flow conditions around the reattachment point, both with and without free-stream turbulence. This sets the scene for the presentation in §3 of the data obtained (in both cases) in the developing boundary layer beyond reattachment. Section 4 provides some further analysis and discussion, §5 describes briefly the results of some numerical computations and the conclusions are summarized in §6.

2. Experimental arrangements

A detailed description of the experiments is given in Castro & Epik (1996, hereafter referred to as CE); only the salient details are repeated here. Figure 1 shows the set-up in the 0.76×0.6 m working section of the 'B' wind tunnel in the Department of Mechanical Engineering, University of Surrey. A trailing-edge flap was used to control the circulation around the whole assembly. In the case of no free-stream turbulence (NFST) it was set to yield no circulation around the entire flat plate assembly and, in the free-stream turbulence case (FST), a slight adjustment was made to force the length of the separated region to be the same as for the NSFT case (such adjustments lead to small changes in the angle of attack of the plate). For the FST case, a standard bi-planar grid was positioned upstream so that the (measured) longitudinal turbulence intensity (u'/U_r) and integral scale (L_x) ranged, respectively, from 5.1% and $3.2h$ at the leading edge to 2.8% and $4.8h$ at the most downstream measurement station ($x = 154h$, with x measured from the plate's leading edge). h is the plate thickness, 9.6 mm, and U_r is a reference velocity, usually about 10 m s^{-1}, measured in the free-stream at $x = 130$ mm (somewhat beyond reattachment at $x = 74$ mm). Spatial correlation measurements showed that, typically, L_x was about $0.9L_\epsilon$, where L_ϵ is the dissipation length scale defined as $L_\epsilon = 1.5(\overline{u^2})^{3/2}/\epsilon$, and the lateral integral scales were about $0.55L_x$. The grid turbulence in these and other respects was closely similar to 'standard' flows generated this way (e.g. Compte-Bellot & Corrsin 1966).

Standard hot-wire and pressure measurement techniques were used throughout, with all instruments interfaced to microcomputers via appropriate i/o cards. For turbulence stresses and higher-order moments, crossed-wire probes were calibrated in yaw using the effective cosine law method (Bradshaw 1971). Errors in measurement are believed to be no greater than those generally obtainable with sufficiently careful use of such techniques. Near reattachment local turbulent intensities were of course too high for sensible use of hot-wire anemometry; in this region pulsed-wire techniques were used. Surface skin friction was determined using surface static tappings and Preston tubes of various diameters, with Patel's (1965) universal calibration. Since it was anticipated that the usual log-law would develop only slowly beyond reattachment, the final C_f data were obtained from smoothed curves drawn through the data from the smallest tube, whose diameter was below 25 wall units in every case. Nonetheless, differences between the data obtained from tubes whose sizes differed by a factor of nearly 2 were always below about 5%.

For both cases the flow around reattachment was found to be adequately two-dimensional over a central span whose width exceeded 16 boundary layer thicknesses. Although there was a noticeable curvature in the reattachment line the variation in x_r did not exceed about 10% over this central region. Such a test is actually a very sensitive measure of three-dimensional effects; checks further downstream showed that the variations of skin friction, C_f, were much smaller over a similar span. Despite these acceptably small deviations, the flow cannot of course be strictly two-dimensional and, with growth of the sidewall boundary layers, must become increasingly less so with

https://doi.org/10.1017/S0022112098002420 Published online by Cambridge University Press

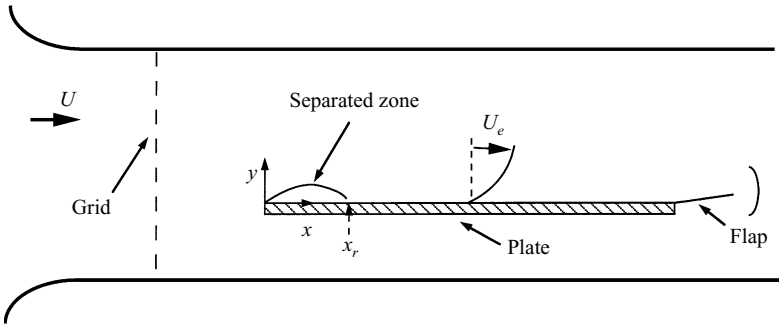


FIGURE 1. Sketch of experimental arrangement.

increasing fetch (x). However, we believe the inevitable three-dimensionality is nonetheless sufficiently weak that it does not significantly affect the flow structure and, in particular, the differences between the two flows and standard zero-pressure-gradient boundary layers. Although there were also, necessarily, axial pressure gradients in the leading-edge region, the surface static pressure data showed that for $x/x_r > 2$ the pressure gradient parameter $(\rho/\nu u_\tau^3)(\partial p/\partial x)$ was below 0.001, so that pressure gradient effects were negligible beyond that point.

In both the NFST and the FST cases the mean length of the separation region, as determined on the spanwise centreline by a surface-mounted twin-tube technique, was $7.7h$ (i.e. $x_r = 74$ mm). (This device has always been found to yield good estimates of the mean reattachment point via comparisons with, for example, surface pulsed-wire techniques or flow visualization.) $x_r/h = 7.7$ is a rather longer 'bubble' than found by other workers – both Cherry *et al.* (1984) and Kiya & Sasaki (1983), for example, had $x_r = 5h$ (with no stream turbulence). However, in both these latter experiments the tunnel blockage was substantially larger (4–5%, cf. the present 1.2%) and, more importantly, the spanwise aspect ratio, W/h, was very much smaller (about 10, cf. 64 in the present case). Spanwise aspect ratio has been shown to have a large effect on the length of nominally two-dimensional separated regions (Hancock & Castro 1993) and the present result is consistent with the trends found in earlier work. Reynolds number, Re, can also have an effect and we note that in this case Re (based on the thickness of the blunt plate and the free-stream velocity) was about 6500, so that the details of the separated region were probably not identical to those which would pertain at much higher Re (see later). However, the flow at reattachment was undoubtedly fully turbulent and was significantly different in the two cases, which was the major objective.

It has been shown previously that reattachment flows have features similar to plane mixing layers distorted by curvature, approach to a plane wall and entrainment of turbulent fluid on the low-velocity side (e.g. Chandrsuda & Bradshaw 1981; Castro & Haque 1987). Since the reattachment flow can in some senses be thought of as providing the initial conditions for the developing boundary layer, it is pertinent to compare the present flow at $x = x_r$ with previous work, partly in order to clarify the different 'starting condition' for the developing boundary layers in the two cases (NFST and FST). Because the scale of the separated region is small (necessary, so that measurements could be made far downstream), no attempt was made to obtain detailed data within it. However, mean velocity and stress profiles were measured at $x = x_r$ in the two cases. The former showed that the flow thickness, δ, defined as the distance to the point where the mean velocity reached 99% of its maximum (free stream) value, was 19.8 mm ($2.06h$) and 22.9 mm ($2.39h$) in the NFST and FST cases,

https://doi.org/10.1017/S0022112098002420 Published online by Cambridge University Press

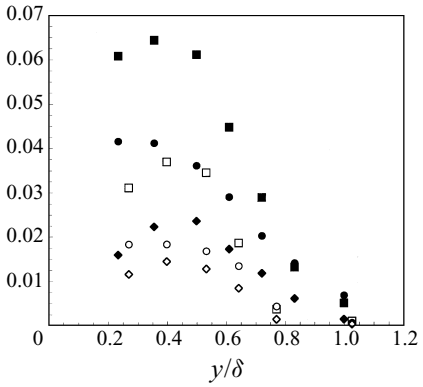


FIGURE 2. Reynolds stresses (normalized by U_r^2) at $x = x_r$ (74 mm). □, $\overline{u^2}$; ○, $\overline{v^2}$; ◇, $\overline{uv}$. Open symbols, NFST; solid symbols, FST.

respectively. This level of stream turbulence thus produced a 16% increase in flow thickness.

Figure 2 shows the Reynolds stress profiles at reattachment ($x_r = 74$ mm). Note first that the maximum stresses are much larger in the FST case. The differences are considerable: $\overline{u^2_{max}}$ and $\overline{uv}_{max}$, for example, are increased by factors of about 1.8 and 2, respectively, with the addition of free-stream turbulence. These are much larger increases than those found in the context of the flow behind a normal flat plate plus splitter plate combination (Castro & Haque 1988). Indeed, in that case the maximum shear stress at reattachment was actually reduced a little by external turbulence. However, it was also shown that free-stream turbulence increases the rate at which the maximum stresses rise from separation to reattachment but leads to a (roughly 20%) shorter bubble. Hillier & Cherry (1981) found that, for the same configuration as the present case, free-stream turbulence of roughly the level used here led to a 33% reduction in bubble length. In the present case, the downstream flap was adjusted so as to yield the same bubble length. The more rapid rise in maximum stresses would then be expected to lead to much larger values at reattachment, as is observed. This was, in fact, one of the reasons for maintaining the same bubble length; we wished in part to identify the extent to which the development rate of the downstream boundary layer is dependent on the 'initial' conditions.

Secondly, it should be noted that the stresses in the absence of free-stream turbulence are lower than those found by Kiya & Sasaki (1983). Their measurements yielded values for $\overline{u^2_{max}}$, $\overline{v^2_{max}}$ and $\overline{uv}_{max}$ of 0.0625, 0.04 and 0.02, respectively, when normalized by the maximum axial velocity at $x = x_r$. Figure 2 suggests corresponding values around 0.038, 0.018 and 0.014 in the present case. This difference is probably partly a Reynolds number effect. The present measurement at $x = x_r$ were obtained with $Re = 3680$, because of the upper velocity limit (about 6 m s^{-1}) on the miniature pulsed-wire probe. Hancock (1995) has shown that, in the flat plate plus splitter plate case, an increase in Re from 3600 to 14000 leads to an increase of about 28% in the maximum axial stress at reattachment, probably because transition in the separated shear layer occurs earlier. Further increases may occur for higher Re; Hillier & Cherry found that the bubble shrank as Re was increased from 27000 to 34000 (and was then unchanged for higher Re) and this would certainly be consistent with increasing stress levels. At the Reynolds number (6500) used for all the present boundary layer measurements it is therefore possible that the stresses at $x = x_r$ in the NFST case were actually somewhat higher than those in figure 2 but, on the basis of Hancock's data, probably

https://doi.org/10.1017/S0022112098002420 Published online by Cambridge University Press

not by more than a factor of around 1.12. In the FST case, such an increase would seem rather less likely, since free-stream turbulence will tend to reduce Reynolds number effects by promoting rather earlier transition. In any event, there is no doubt that the 'initial condition' for the developing boundary layer is considerably different in the two cases in that, although the flow thickness is similar, the stress levels are certainly not.

3. Results and initial discussion

3.1. *The mean flow*

The downstream variations of mean surface skin friction (which is zero at reattachment) and boundary layer shape parameter are given in CE, where it was shown that the general form of the development process is similar in both cases. By the final measurement station in the NFST case C_f and H are both within 5% of their normal values (at the appropriate momentum thickness Reynolds number), but the Clauser parameter, $G = (2/C_f)^{1/2}(H-1)/H$, is still, at $G = 5.9$, considerably below the standard (Coles') value of 6.8.

There is considerable evidence in the literature that subsequent to reattachment mean velocity profiles have a significant dip below the standard log law. This was first noted by Bradshaw & Wong (1972) and our data are typical in this respect. Figure 3 shows axial velocity profiles plotted in the usual wall units, for both the NFST and the FST cases. The shear velocity (u_τ) was obtained from the Preston-tube skin friction data as explained earlier. (For these and all subsequent profiles, the free-stream reference velocity used is the *local* maximum velocity. We refer to this as U_e throughout this paper; there is roughly a 3% increase in U_e between $x = 130$ mm and the final measuring station at $x = 1480$ mm). It is immediately clear from figure 3 that even some $0.8x_r$ beyond the mean reattachment point (i.e. $x = 130$ mm, $x/x_r = 1.76$) – the first measurement station – the usual log law does not exist. In fact there is little evidence of its emergence until at least $x/x_r = 3$, emphasizing the slowness of the development process which, nonetheless, is rapid compared with the development of the outer region of the flow (see later). This may be further evidence of the relative robustness of the log law which, as is well-known, often survives (or, in this case, appears) in situations where one might not strictly anticipate its validity. In any case, the turbulence quantities do not develop their canonical form in the inner region as quickly as the mean flow (see §3.2). It is also clear that stream turbulence does not initiate a more rapid development of the log law. This is emphasized by figure 4, which shows the percentage deviation (in u^+) from the log law at two values of y^+ (100 and 250), plotted as a function of distance from reattachment normalized by the shear layer thickness there. We will hereafter call this latter parameter x' ($x' = (x-x_r)/\delta_r$), with δ_r the flow thickness at $x = x_r$. Table 1 lists the values of x, x/x_r and x' at which most of the data were obtained for the two cases.

At $y^+ = 100$ the rate at which u^+ returns to its standard value is independent of the state of the free stream, at least within the experimental uncertainty. Note that in this work we define the 'standard' log law by $\kappa u^+ = \log(y^+) + \kappa A$, with $\kappa = 0.4$ and $A = 5.1$ (and $u^+ = u_\tau, y^+ = yu_\tau/\nu$). These values are those used by Fernholz & Finley (1996) in their recent comprehensive review of zero-pressure-gradient boundary layers. The alternative pair sometimes used (0.41, 5.2) would reduce deviations (at $y^+ = 100$) by about 1% whereas the pair (0.4, 5.0), which has some theoretical justification (Phillips 1994), would reduce deviations by a mere 0.5%.

Further away from the wall ($y^+ = 250$), but still (just) within the region which would

https://doi.org/10.1017/S0022112098002420 Published online by Cambridge University Press

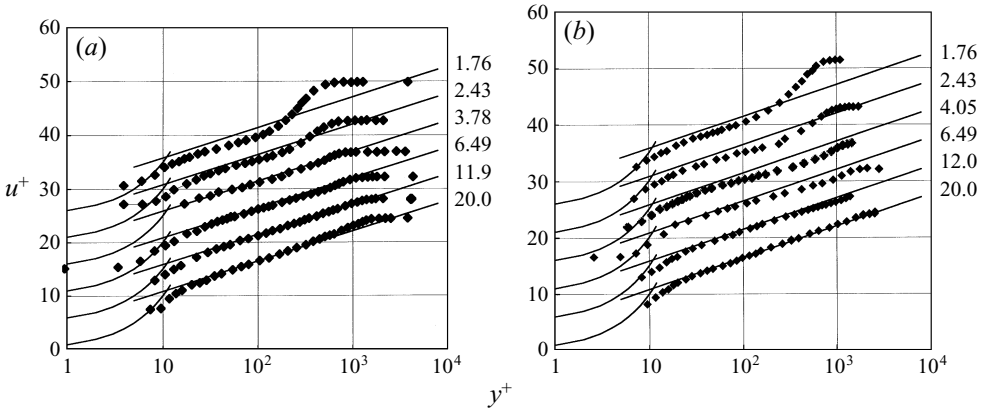


FIGURE 3. Mean velocity profiles: (*a*) NFST, (*b*) FST. Note shift of abscissa by five units for each set. x' values are shown, from top to bottom; corresponding values of x (mm) and x/x_r are given in table 1.

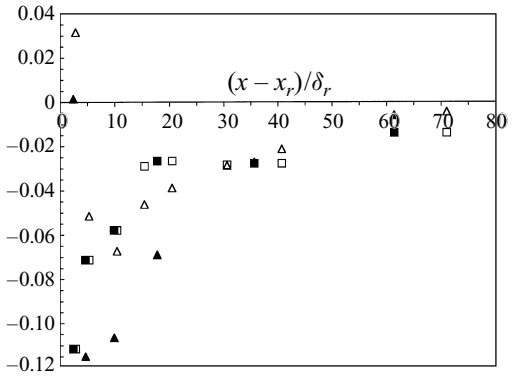


FIGURE 4. Percent deviation in u^+ from standard log law. □, $y^+ = 100$; △, $y^+ = 250$. Open symbols, NFST, solid symbols, FST.

NFST, $\delta_r = 19.8$ mm			FST, $\delta_r = 22.9$ mm		
x (mm)	x/x_r	$x' = (x-x_r)/\delta_r$	x (mm)	x/x_r	$x' = (x-x_r)/\delta_r$
130	1.76	2.83	130	1.76	2.45
180	2.43	5.35	180	2.43	4.63
280	3.78	10.4	300	4.05	9.87
480	6.49	20.5	480	6.49	17.7
880	11.9	40.7	890	12.0	35.6
1480	20.0	71.0	1480	20.0	61.4

TABLE 1. Axial measurement stations for the two flows.

normally be described by the log law (at these momentum thickness Reynolds numbers of > 2000), the initial behaviour of the deviation is noticeably different in the two cases. In the FST case, the 'dip' below the log law appears to propagate outwards from the wall so that the maximum deviation is significantly greater than it is for the NFST case – by almost a factor of 2; this is almost certainly a result of the much higher initial turbulence energy in the flow at reattachment rather than a direct influence of stream

https://doi.org/10.1017/S0022112098002420 Published online by Cambridge University Press

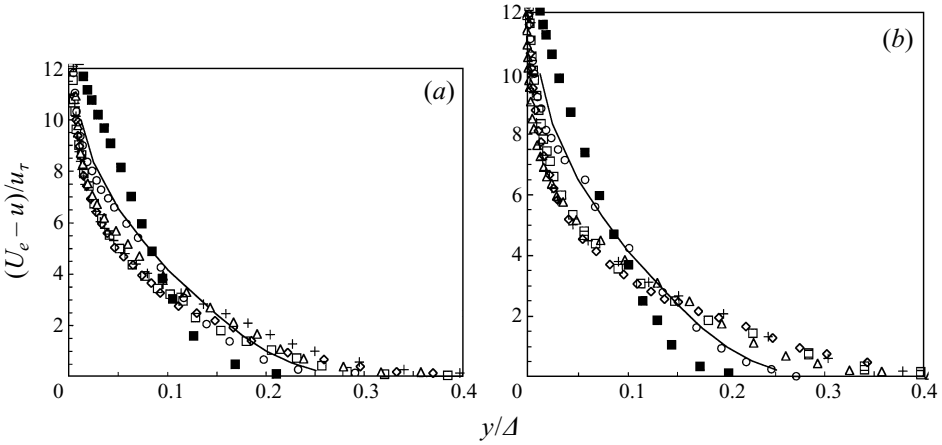


FIGURE 5. Mean velocity profiles in outer layer scaling. (*a*) NFST: ■, $x' = 2.83$; ○, 5.35; △, 10.4; +, 20.5; ◇, 40.7; □, 71. (*b*) FST: ■, $x' = 2.45$; ○, 4.63; △, 9.87; +, 17.7; ◇, 35.6; □, 61.4. See table 1 for corresponding x and x/x_r values.

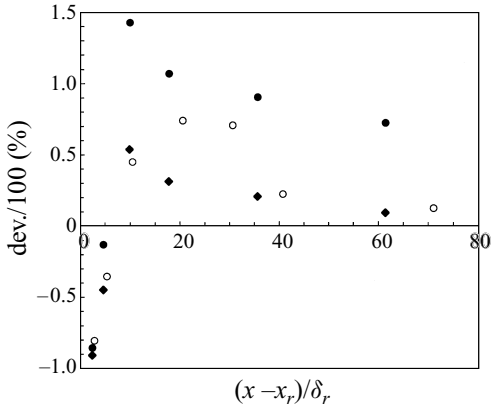


FIGURE 6. Percent deviation of $(U_e-u)/u_\tau$ from standard outer-layer profile. ○, NFST; ●, FST. ◆, FST, using as reference Hancock's outer-layer profile for the case $u'/U_e = 0.0255$, $L_e/\delta = 0.77$.

turbulence. After the initial recovery (beyond about $x' = 30$, say) there is little difference in the deviation from the log law between the two cases. At the last measurement station the deviation has fallen to around 1 % in both cases; it is actually a little smaller than the deviation at $y^+ = 100$, but the difference is probably within the experimental uncertainty. We conclude that as far as the inner region is concerned, beyond the first 10–20 boundary layer thicknesses from reattachment the rate at which it develops towards normality is largely independent of the nature of the external stream. Things are rather different in the outer part of the flow, as we now demonstrate.

Figure 5 shows the velocity profiles in outer layer coordinates, where wall distances are normalized by the Rotta scaling parameter defined by $\Delta = \delta^*/u^+$ (where δ^* is the usual displacement thickness). The standard wake-law profile is included and it is clear that the development of the outer layer is non-monotonic, in the sense that the values of $(U_e-u)/u_\tau$ (at a fixed y/Δ beyond about 0.15, say) start below normal but rapidly overshoot before relaxing slowly back to normality. This is illustrated explicitly in figure 6. Note that unlike the wall-law deviations in the inner layer, the wake-law

https://doi.org/10.1017/S0022112098002420 Published online by Cambridge University Press

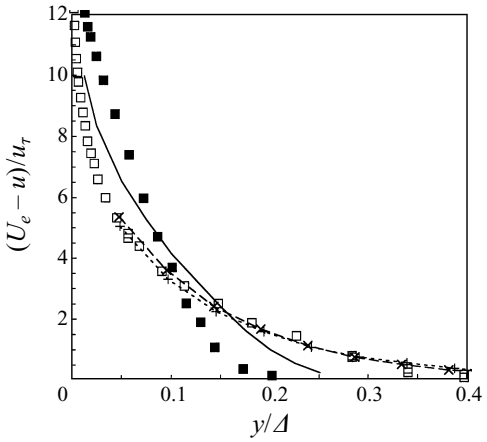


FIGURE 7. Mean velocity profiles, FST: ■, x (mm) = 130, $x' = 2.45$; □, 1480, 61.4. ——, standard boundary layer. Hancock (1980) cases: ——×——, $u'/U_e = 0.0255$, $L_e/\delta = 0.77$; ——+——, 0.0399, 1.15.

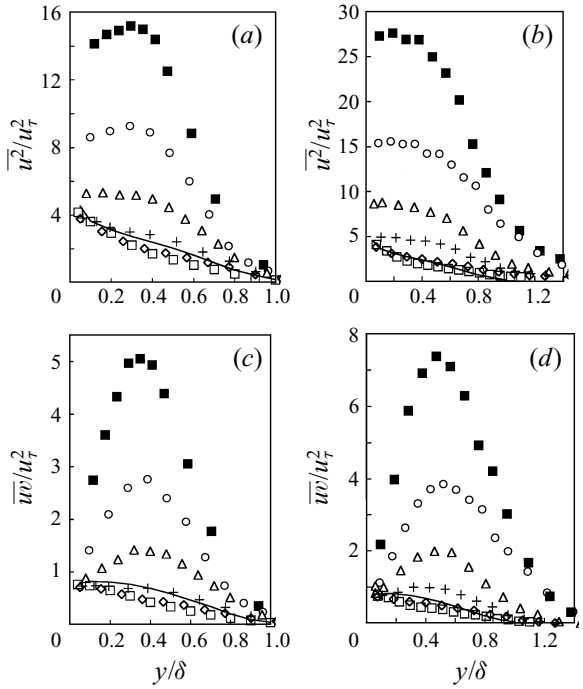


FIGURE 8. Reynolds stresses, normalized by u_τ^2. (a, c), NFST; (b, d), FST. (a, b) $\overline{u^2}$, (c, d). $\overline{uv}$. Legend as in figure 5. ——, Standard boundary layer.

deviation is not expected to recover to zero in the FST case. Stream turbulence causes a reduction or even, for high enough intensities, a complete collapse of the wake region and figure 7 compares the results (at $x' = 2.45$ and 61.4) with Hancock's (1980) data for his two cases closest in intensity and length scale ratio to the present FST values. It is interesting that at $x' = 61.4$, where $u'/U_e = 0.026$ and $L_e/\delta = 0.44$, not just the outer flow but the entire velocity profile is very similar to that obtained by Hancock.

https://doi.org/10.1017/S0022112098002420 Published online by Cambridge University Press

If the outer law deviation from the Hancock result for $u'/U_e = 0.0255$ and $L_e/\delta = 0.75$ (rather than from the standard wake-law) is calculated, the rate of development is actually rather faster than in the NFST case; these deviations are included in figure 6. We will hereafter refer to this latter Hancock case as the 'HB reference case'.

At the final measurement station in the FST case the normalized differences in surface skin friction and shape factor from standard boundary layer values at the same Re ($\Delta C_f/C_f = 0.138$ and $\Delta H/H = 0.070$) are close to, but not the same as, the values for this Hancock reference case (0.148 and 0.065, respectively). The differences, although small, are consistent with the flow not having reached the state it would 'normally' be in under stream turbulence of this intensity. Although the FST value of L_e/δ (0.44) is lower than the Hancock value (0.75), Hancock's results show that this would normally lead to larger skin friction and shape factor deviations, whereas our value for the former is measurably smaller. In fact, for the present FST parameters at this final measurement station Hancock's correlation suggests $\Delta C_f/C_f = 0.157$, $\Delta H/H = 0.073$. However, although the mean flow is certainly different from this HB reference case, the difference does seem smaller than the difference between the NFST case and a standard boundary layer (e.g. figure 6). It is arguable that stream turbulence will enhance the rate at which the outer flow 'forgets' its complex early history, at least in cases (as here) where the stream turbulence length scale is of the same order as the boundary layer thickness. Further discussion of this point is given later.

3.2. *Turbulence quantities*

3.2.1. *Stresses*

All four non-zero components of the turbulence stresses (along with third- and fourth-order moments) were measured at eight stations downstream of reattachment between $x = 130$ mm and $x = 1480$ mm. Stress data for the NFST case were presented in CE. Here we present in figure 8 a selection of these alongside the corresponding data for the FST case. The figure shows the axial stress and the shear stress variations, normalized by u_τ^2 to allow sensible comparison with standard boundary layer data. We have chosen to use the Erm & Joubert (1991) measurements (at $Re_\theta = 2788$) for the latter, as these are representative of modern, high-quality data (Fernholz & Finley 1996). Ideally, of course, it would have been best to obtain such data in our own facility but given the high spanwise aspect ratio of our flows, the negligible axial pressure gradient and the well-proven instrumentation techniques, there is no reason to believe that such data would be significantly different from those obtained by Erm & Joubert.

In the earliest stages of development (i.e. upstream of $x = 130$ mm) all the stresses except $\overline{w^2}$ have maxima remote from the wall – recall figure 2 for profiles at reattachment. This is symptomatic of the mixing-layer-like flow around reattachment (see CE) and reasons for the continual increase in $\overline{w^2}$ all the way to the wall around reattachment have been explained by Castro & Haque (1987). In the absence of stream turbulence the maximum in $\overline{u^2}$ gradually disappears and is not apparent by $x' = 10.4$ (figure 8*a*). However, with stream turbulence this process is significantly more rapid – figure 8(*b*) shows that there is no maximum beyond $x' = 2.45$. In contrast, the maxima in $\overline{v^2}$ (not shown) and $\overline{uv}$ (figure 8*c*, *d*) take much longer to disappear whether or not stream turbulence is present – by soon after $x' = 26$ in the case of $\overline{v^2}$ although a little earlier for $\overline{uv}$. The general behaviour of the turbulence stresses is consistent with that found by Alving & Fernholz (1996) downstream of a reattaching axisymmetric boundary layer. They noted that $\overline{v^2}$ and $\overline{uv}$ retain the peaks they have around reattachment for much longer than the other two components and commented that this behaviour is, in fact, a common feature in other flows developing subsequent to

https://doi.org/10.1017/S0022112098002420 Published online by Cambridge University Press

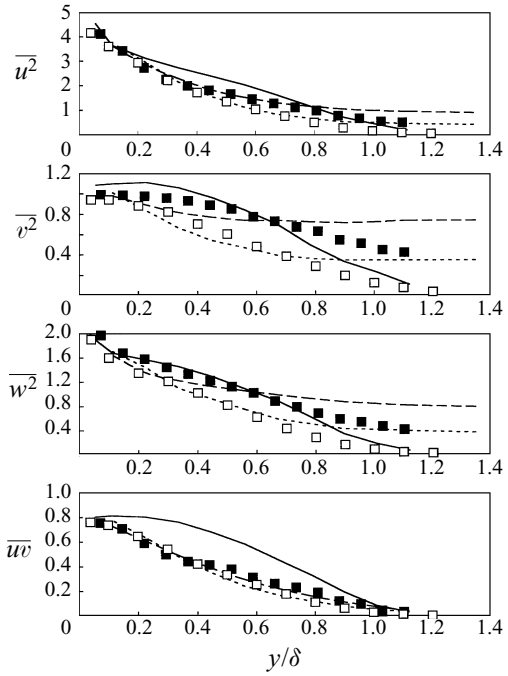


FIGURE 9. Reynolds stresses, normalized by u_τ^2, at $x = 1480$ mm. Open symbols, NFST; solid symbols, FST. ——, Standard boundary layer. Hancock (1980) cases: – – – –, $u'/U_e = 0.0255$, $L_e/\delta = 0.77$; — — —, 0.0399, 0.82.

reattachment and is largely independent of the nature of the flow upstream of separation.

A particularly significant feature of the results is that all the stresses eventually fall below standard boundary layer values except perhaps in the inner region (below $y/\delta = 0.1$, say). This is demonstrated more clearly in figure 9, where profiles of all stresses at the final measurement station are compared with the standard (Erm & Joubert) data and with the HB reference case. Notice in particular that the shear stress profiles have by that stage fallen well below the standard curve and that the addition of stream turbulence makes virtually no difference to the profile at this station. It is clear that all the stress components for the NFST case are close to the HB case (except of course towards the outer edge of flow where the normal stresses in the latter approach the levels appropriate to the imposed free-stream turbulence). Figure 9 also includes stress data for the Hancock case having stream turbulence parameters similar to those at $x' = 2.45$ in the present case (i.e. the first measurement station downstream of $x' = 0$). Although both $\overline{u^2}$ and $\overline{uv}$ profiles in the FST case are similar to these data, the other stress components are not. There is, of course, no reason why one should expect agreement but the Hancock data do demonstrate that for length scale/boundary layer thickness ratios similar to those of the present case, higher stream intensity levels lead to higher normal stresses, particularly $\overline{v^2}$ and $\overline{w^2}$, although all the stresses remain lower than standard values (at least for $y/\delta < 0.6$). Following the CE argument that, in the NFST case, the outer flow acts rather like stream turbulence, the higher initial stresses in the FST case would then be 'equivalent' to even higher stream turbulence; the data in figure 9 are in that sense consistent with the trends in the two Hancock cases.

https://doi.org/10.1017/S0022112098002420 Published online by Cambridge University Press

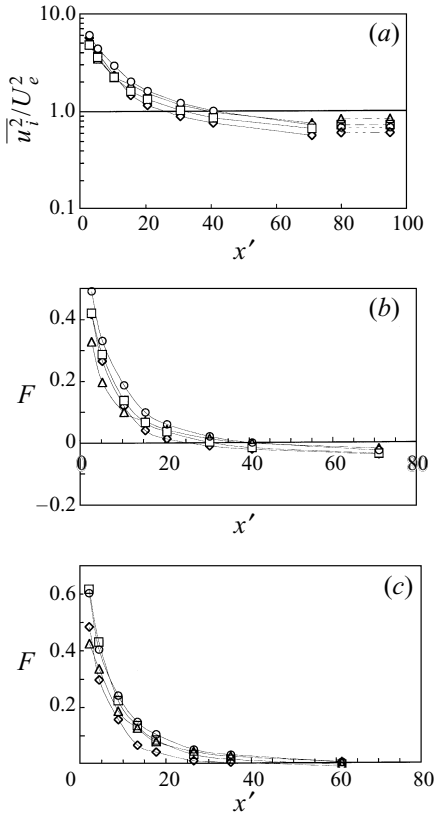


FIGURE 10. Development of stresses at $y/\delta = 0.5$. (*a*) NFST, values divided by standard boundary layer values: □, $\overline{u^2}$; ○, $\overline{v^2}$; △, $\overline{w^2}$; ◇, $\overline{uv}$ (all normalized by U_e^2). Values at right refer to the HB reference case. (*b*) NFST and (*c*) FST: □, F_u; ○, F_v; △, F_w; ◇, F_{uv}.

The rate at which the stresses in the outer flow fall with downstream distance, for the NFST case and typified by the behaviour at $y/\delta = 0.5$, is shown in figure 10(*a*), where the stresses (normalized by U_e^2 rather than u_τ^2) are plotted as ratios with their standard values. A logarithmic scale is used to emphasize the behaviour near unity. It is noticeable that $\overline{uv}$ and $\overline{u^2}$ fall below the standard values rather earlier than do $\overline{v^2}$ and $\overline{w^2}$, i.e. by $x' = 25$ and 30 (for $\overline{uv}$ and $\overline{u^2}$, respectively) compared with around $x' = 40$ (for $\overline{v^2}$ and $\overline{w^2}$). The figure includes the corresponding ratios for the HB reference case and it is evident that by the final measurement station all the stress ratios have fallen to values marginally below these although eventually (sufficiently far downstream) they must recover to unity.

A more appropriate way to compare the initial rates of decay is to compute the fractional decrease in stress; this is defined (for the axial component, say) by

$$F_u = (\overline{u^2} - \overline{u_s^2})/(\overline{u_r^2} - \overline{u_s^2}),$$

where $\overline{u^2}$, $\overline{u_r^2}$ and $\overline{u_s^2}$ are the stress values at the local position (x'), at the reattachment ($x' = 0$) and for a standard boundary layer, respectively, and again all normalized by U_e^2. F_u, F_v, F_w and F_{uv} are shown in figures 10(*b*) and 10(*c*) for the NFST and FST cases, respectively. In both flows the lateral stress component ($\overline{w^2}$) initially falls significantly more rapidly than the others (all curves must start at unity for $x' = 0$). This is perhaps not surprising. The influence of the wall on the mixing-layer-like flow farther upstream

https://doi.org/10.1017/S0022112098002420 Published online by Cambridge University Press

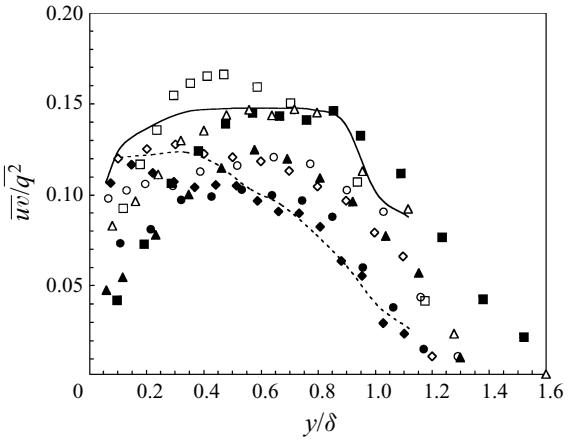


FIGURE 11. Profiles of $\overline{uv}/\overline{q^2}$. Open symbols, NFST; solid symbols, FST: □, x (mm) = 130; △, 280; ○, 480; ◇, 1480. ——, Standard boundary layer; – – – – –, HB reference case ($u'/U_e = 0.0255$, $L_e/\delta = 0.77$).

begins prior to reattachment and is most noticeable in preventing the other two normal stresses rising as much as they otherwise would (Castro & Haque 1987); the re-entrainment process upstream of reattachment enhances particularly $\overline{w^2}$, so it is natural that its removal (by reattachment) leads initially to a more rapid fall in this component than in the others.

A further point to note about these data is that they imply an extremely long development length; figure 10 suggests that none of the stresses (in either case) have quite fallen to their minimum by the final station. A considerably greater downstream distance would apparently be required before the stresses (in the NFST case) rise again to their standard values or (in the FST case) fall to values appropriate for a boundary layer beneath stream turbulence. This conclusion is consistent with the implication of the velocity profile data (e.g. figure 7) which, even at the final measurement station and although the log law is by then fully established, remain very different from the standard boundary layer (or, in the FST case, the boundary layer beneath stream turbulence). It is also consistent with the behaviour of turbulence structural parameters like $\overline{uv}/\overline{q^2}$. Figure 11 shows a selection of profiles of $\overline{uv}/\overline{q^2}$ for both flows at various downstream stations. In the absence of stream turbulence the initial profile (at $x =$ 130 mm) is similar to that for a plane mixing layer, in that it has a rather higher maximum than in a standard boundary layer and falls on both edges of the flow. By the final measurement station, even in the inner region ($y/\delta < 0.2$) the shear stress has only just about developed sufficiently to yield $\overline{uv}/\overline{q^2}$ values similar to those in the inner half of a standard boundary layer. (They are actually rather closer at this stage to those in the HB reference case.) In the outer half of the layer there is still considerable development yet to occur at the last station ($x = 1480$ mm). With stream turbulence, although the outer half of the layer eventually has a $\overline{uv}/\overline{q^2}$ profile similar to the HB reference case, the inner half remains under-developed. Alving & Fernholz (1996) also noticed this very slow shear stress recovery in the inner half of the flow. The development is even slower in the present case, although it must be remembered that the distortion is more overwhelming so this is to be expected; Alving's measurements did not extend beyond about $x' = 20$ (in the present notation) compared with about 70 in the present case, so it is not known how complete recovery would have been by $x' = 70$ in their case.

https://doi.org/10.1017/S0022112098002420 Published online by Cambridge University Press

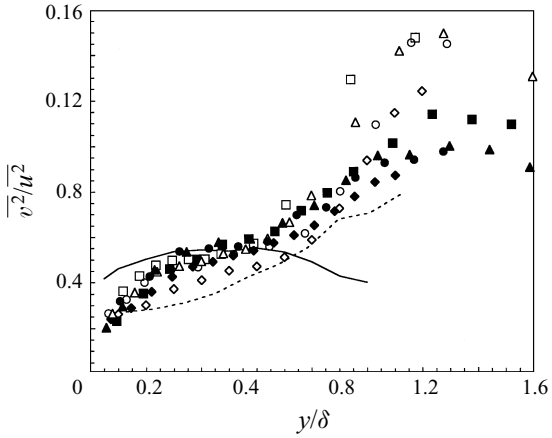


FIGURE 12. Profiles of $\overline{v^2}/\overline{u^2}$. Legend as for figure 11.

Similar behaviour is observed in the other stress ratios. We show in particular, in figure 12, $\overline{v^2}/\overline{u^2}$. Here again, at $x = 1480$ mm $\overline{v^2}$ is still significantly lower relative to $\overline{u^2}$ in the inner half of the flow ($y/\delta < 0.7$) than in a standard boundary layer. Further outboard the ratio is larger than in a standard boundary layer, as found for boundary layers beneath stream turbulence where it must approach (roughly) unity in the free stream. The implication of all this is clear: the turbulence structures in the outer flow remain very different to standard outer-layer structures in a boundary layer and have a considerable influence on the behaviour of the inner part of the developing boundary layer.

3.2.2. *Higher-order moments*

As an example of the velocity triple-product measurements, figure 13 shows profiles of normalized $\overline{u^3}$, $\overline{u^2v}$, $\overline{uw^2}$, $\overline{v^3}$, $\overline{uw^2}$, $\overline{u^2w}$ and $\overline{w^3}$ at $x = 130$ and 1480 mm for both flows ($\overline{v^2w}$ and $\overline{vw^2}$ were not measured). For truly two-dimensional flows and assuming negligible instrument errors $\overline{u^2w}$ and $\overline{w^3}$ should be zero. The figure shows that these were indeed generally very small compared with the other components; of the examples shown, figure 13(*a*) has the largest values but these are not typical. Two sets of $\overline{u^3}$ data were obtained at each station (with the cross-wires in two orthogonal planes) and the agreement between them is satisfactory in all cases. Note firstly that at $x = 130$ mm (i.e. $x' < 3$) the profile shapes are similar to those on the high-velocity side of regular plane mixing layers, although the numerical values are substantially higher. The maximum (negative) value of $\overline{u^3}$, for example, is roughly twice and four times what it would be in a mixing layer, for the NFST and FST cases, respectively. Near the wall most profiles show a change of sign and the values must then eventually fall to zero again at the wall. Because of the reattachment process and the wall influence, they do not develop the large peaks that occur on the low-velocity side of a plane mixing layer (which have roughly the same magnitudes as the oppositely-signed peaks further outboard). This low-velocity side of the upstream mixing layer (bounding the separated region) is effectively 'cut-off' around reattachment.

Far downstream the triple-products have all fallen very substantially (figures 13*c* and 13*d*), reaching maxima not too dissimilar to those in a standard boundary layer. (Note the very large change in scales in these figures – peak values typically fall by nearly two orders of magnitude between $x = 130$ mm and 1480 mm). However, the profile shapes are still very different to those found either in a standard boundary layer

https://doi.org/10.1017/S0022112098002420 Published online by Cambridge University Press

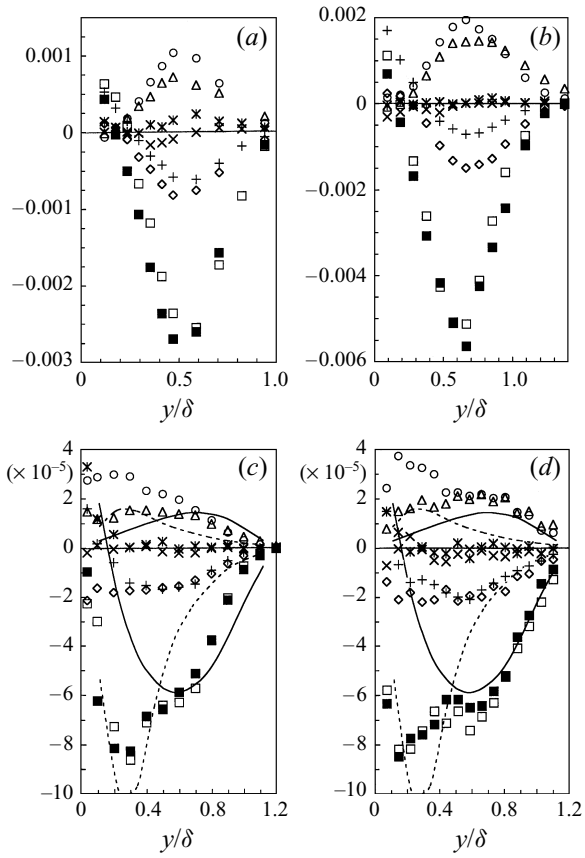


FIGURE 13. Triple velocity products at $x = 130$ mm (*a*, *b*) and 1480 mm (*c*, *d*). NFTS (*a*, *c*); FST (*b*, *d*). □, ■, $\overline{u^3}$; ○, $\overline{u^2v}$; ◇, $\overline{uv^2}$; △, $\overline{v^3}$; +, $\overline{uw^2}$; ×, $\overline{u^2w}$; ∗, $\overline{w^3}$. ——, Standard boundary layer and – – – – –, HB reference case ($u'/U_e = 0.0255$, $L_e/\delta = 0.77$) for $\overline{u^3}$ (mostly −ve values) and $\overline{v^3}$ (+ve values). All values normalized by U_e^3.

or in the HB reference case. The largest differences occur in the region $y/\delta < 0.6$ where, for $\overline{u^3}$ for example, a peak is reached (around $y/\delta = 0.3$ in the NFST case), just as it is for the HB reference case. There is clearly considerable flow development still to occur and these data confirm once again that a very substantial downstream fetch would be required before standard boundary layer profiles would be recovered.

It is interesting that although the numerical values at $x = 130$ mm for the NFST and FST cases differ so much (cf. figures 13*a* and 13*b*), by $x = 1480$ mm the differences are relatively small (cf. figures 13*c* and 13*d*). Figure 14 shows how rapidly the peak values of $\overline{u^3}$ and $\overline{v^3}$ (as examples) fall with downstream distance. In the FST case the initial value of $\overline{u^3}$ (at $x' = 0$) is significantly higher, relative to the standard boundary layer value, than it is in the NFST case so it is not surprising that the fall is initially more rapid. That these initial values are significantly higher than those typical of a plane mixing layer (included in the figure) emphasizes the turbulence amplification that occurs in the separated region and around reattachment. It is also interesting that in the outer half of the flow the triple products in the NFST case eventually fall below their corresponding levels in a standard boundary layer (see, for example, $\overline{u^3}$ and $\overline{v^3}$ in figure 13*c*). Unlike the Reynolds stresses, however, they do not (at least by the final measurement station) fall to levels as low as those found in the HB reference case but,

https://doi.org/10.1017/S0022112098002420 Published online by Cambridge University Press

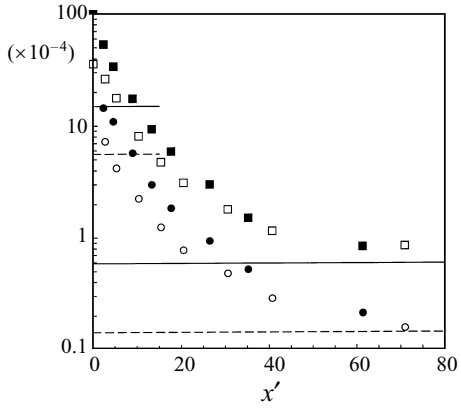


FIGURE 14. Decay of maximum (absolute) values of $\overline{u^3}$ (□, ■) and $\overline{v^3}$ (○, ●). Open symbols, NFST; solid symbols, FST. Standard mixing layer (upper pair) and boundary layer values of peak $\overline{u^3}$ (——) and $\overline{v^3}$ (— — — —).

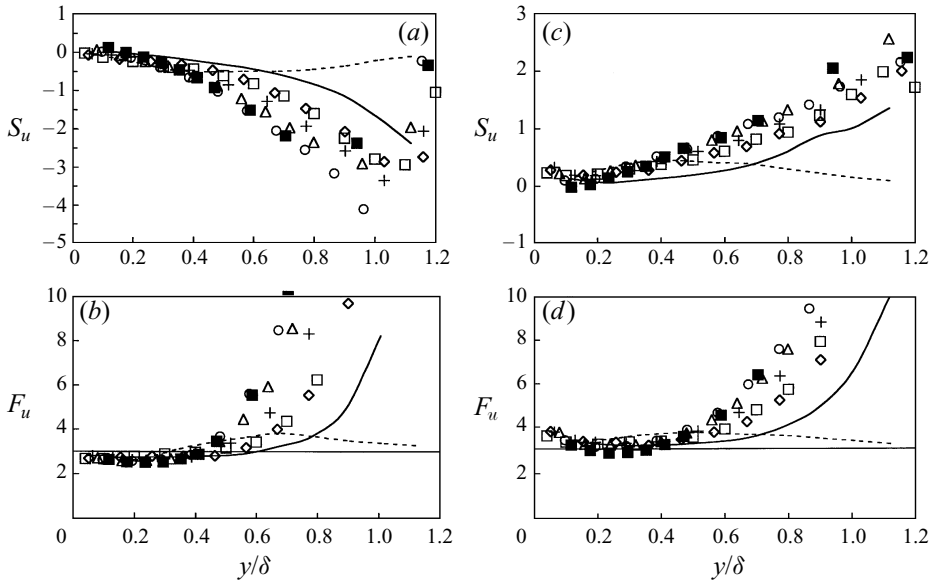


FIGURE 15. Skewness (*a*, *c*) and flatness factor (*b*, *d*) of the axial velocity component. (*a*, *b*), NFST; (*c*, *d*) FST. Legend as for figure 5. – – – – –, HB reference case ($u'/U_e = 0.0255$, $L_e/\delta = 0.77$); ——, standard boundary layer.

nonetheless, there is clearly some non-monotonic behaviour as there is in the case of the second moments. In the inner half of the flow the levels remain very much higher than standard even at $x = 1480$ mm. They are, in fact, similar to those expected in the presence of stream turbulence (compare $\overline{u^3}$ and $\overline{v^3}$ for $y/\delta < 0.4$ with the HB reference data in figure 13*c*). The addition of stream turbulence does not significantly affect this behaviour (figure 13*d*). The implication of these data for the turbulence transport term in the energy and shear stress transport equations is discussed later.

Further indications of the extremely long-lived nature of the flow structures in the outer half of the boundary layer are provided by the skewness and flatness factor data. Samples of these are shown in figure 15. Around reattachment the high flatness and

https://doi.org/10.1017/S0022112098002420 Published online by Cambridge University Press

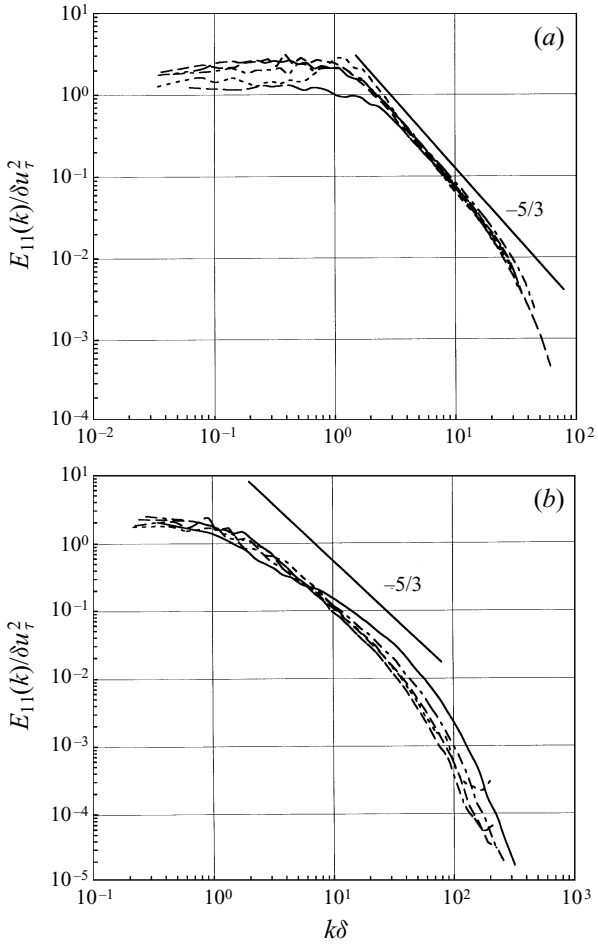


FIGURE 16. u-component energy spectra, NFST. (a) $x = 130$ mm, $x' = 2.83$: ——, $y/\delta = 0.082$; – – – –, 0.35; — — —, 0.65; --- ---, 0.82; – – – – –, 1.0. (b) $x = 1480$ mm, $x' = 71$: ——, $y/\delta = 0.04$; – – – –, 0.16; — — —, 0.4; --- ---, 0.72; – – – – –, 1.0.

strongly negative skewness in the outer half of the flow (compared with standard boundary layer values) are indicative of the more energetic entrainment process typical of plane mixing layers. These high levels are maintained throughout the entire measurement region. In both flows the levels in the inner half of the layer are similar to those found in the HB reference case whereas, in the FST case (figure 15c, d) both the skewness and the flatness in the outer layer have begun to approach the values expected in a boundary layer with stream turbulence. All these trends are followed in the skewness and flatness profiles (not shown) for the other two velocity components.

3.2.3. *Spectra and length scales*

Energy spectra of the axial velocity component were measured at five or six wall distances at most of the axial stations used for the complete profile measurements discussed earlier. Typically, 150–250 blocks of 2048 samples obtained at 10 kHz from suitably filtered single hot-wire signals were appropriately transformed to obtain the spectra. Figure 16 shows the spectral energy density, $E_{11}(k)$, vs. wavenumber, k ($2\pi f/U_c$, where U_c is the local velocity), normalized so that

https://doi.org/10.1017/S0022112098002420 Published online by Cambridge University Press

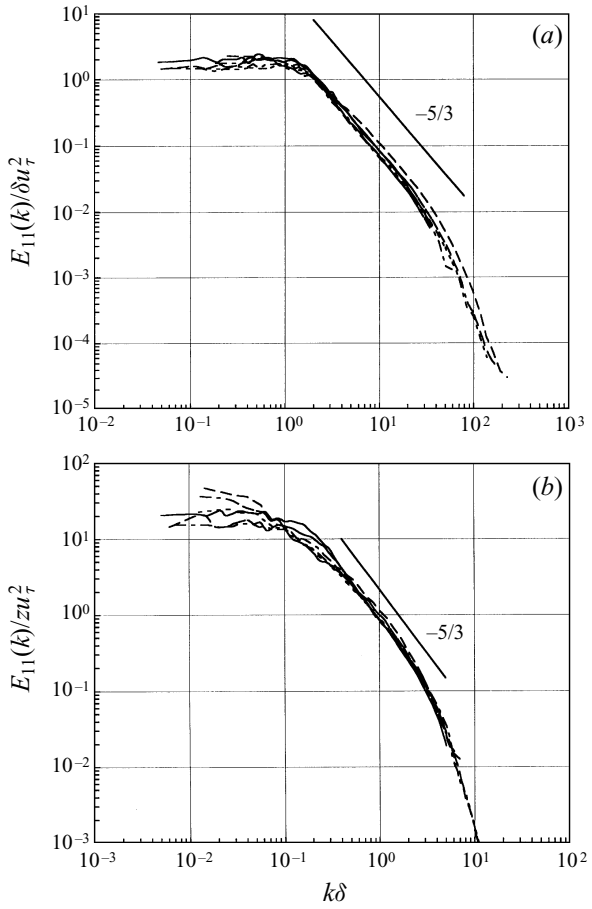


FIGURE 17. u-component energy spectra, NFST. (*a*) Outer layer scaling: ——, $x' = 2.83$, $y/\delta = 0.35$; — — —, 5.35, 0.48; — — —, 10.4, 0.4; — — —, 20.5, 0.45; --— — —--, 40.7, 0.52; — — —, 71, 0.4. (*b*) Inner region scaling: ——, $x' = 2.83$, $y/\delta = 0.082$; — — —, 5.35, 0.096; — — —, 10.4, 0.1; — — —, 20.5, 0.064; --— — —--, 40.7, 0.052; — — —, 71, 0.04.

$$\int_0^\infty E_{11}(k)\,\mathrm{d}k = \overline{u^2},$$

and plotted using outer scaling, i.e. with δ and u_τ as length and velocity scales. Far downstream (figure 16*b*) the spectra have the form expected for a regular boundary layer (Fernholz & Finley 1996). In the inner region and at low frequencies there is evidence of the k^{-1} behaviour expected in what Perry, Lim & Henbest (1986) call the 'overlap' region, i.e. where both inner and outer scaling apply, and at high frequencies the trend with increasing y is as expected. These features are not present at $x' = 2.83$ (figure 16*a*). Here the spectra are much more characteristic of those found in a plane mixing layer – even very close to the wall. The $k^{-5/3}$ region is clearer (because the turbulence Reynolds numbers are significantly higher here than further downstream) and there is reasonable collapse except at low frequencies. There is also a distinct peak around $k\delta = 1$ in the spectrum measured at the outer edge of the flow ($y/\delta = 1$), which is typical for mixing layers and is probably a result of the combination of (relatively) high-energy large-scale motions and the intermittency. This peak has disappeared by $x' = 10.3$ and is not present at all in the FST case. The former is probably a result of

https://doi.org/10.1017/S0022112098002420 Published online by Cambridge University Press

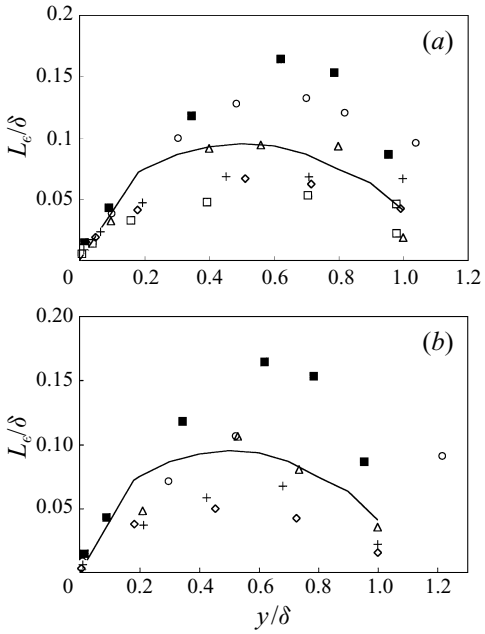


FIGURE 18. Dissipation length scale profiles: (*a*) NFST, (*b*) FST. Legend as for figure 5.

the substantial reduction in turbulent energy that has occurred by that distance downstream (more than a factor of 2, figure 8*a*) whereas the latter must be because the 'non-boundary-layer fluid', which would contain only irrotational fluctuations in the NFST case, is actually turbulent and has a length scale of the same order as the boundary layer thickness.

Figure 17(*a*) shows that around $y/\delta = 0.5$ there is very little change in spectral shape with downstream distance if outer scaling is used. However, in the near-wall region, as noted above, the spectral shape is initially symptomatic of a mixing-layer-like flow dominated by large-eddy motions – the $x' = 2.83$ spectrum plotted using inner scaling in figure 17(*b*) would collapse onto the spectra of figure 17(*a*) if outer scaling were used. Further downstream the spectrum has a form more appropriate for the inner region of a standard boundary layer. Corresponding measurements made in the FST case show that the addition of stream turbulence does little to change the nature of the spectra nor the way they develop, emphasizing once again the dominance of the decaying outer layer structures.

Figure 18 shows profiles of the dissipation length scale, defined by $L_\epsilon = (-\overline{uv})^{3/2}/\epsilon$, for both flows; ϵ was obtained by fitting the spectra to the standard inertial subrange (with the Grant, Stewart & Molliet 1962 value of the subrange constant). There was usually at least half a decade of the spectrum which had an accurate $-5/3$ slope but, nonetheless, this is not a particularly precise means of determining ϵ. However, L_ϵ is close to its expected value of κy in the near-wall region far downstream, where the presence of a log law suggests a reasonable balance between turbulent energy production and dissipation. At the first measurement station there is only a hint of the rather higher length scales first suggested by Bradshaw & Wong (1970) for regions just downstream of reattachment, although the mixing length (not shown) is significantly higher than κy (see CE). Perhaps $x = 130$ mm ($2.83\delta_r$ downstream of reattachment in the NFST case) is a little too far from reattachment to see the more rapid rise in L_ϵ with wall distance that presumably must occur just beyond $x' = 0$.

https://doi.org/10.1017/S0022112098002420 Published online by Cambridge University Press

Further away from the wall the higher length scales certainly decrease very rapidly with downstream distance (in both cases) and beyond $x = 280$ mm the profiles actually fall below the standard boundary layer profile. This may eventually be partly a result of the lower shear stress levels but cannot be explained solely on that basis; at $x =$ 480 mm, for example, the shear stress (whether normalized by u_τ^2 or U_e^2) is still at least as high as standard boundary layer levels across the whole layer. The evidence for unusually high levels of dissipation over most of the flow even at these large distances downstream (around $70\delta_r$) seems strong. In contrast to these data, Hancock showed that stream turbulence did not noticeably affect L_ϵ/δ. However, his measurements were limited to cases in which the free-stream length scale was about twice the boundary layer thickness (so no data are available for the HB reference case) and it is possible that for smaller length scales some differences would have appeared.

4. Further discussion

The large-eddy structures in the reattaching flow around $x' = 0$ are undoubtedly very different from those which occur in a standard boundary layer. They also differ from those in plane mixing layers, which are often characterized by identifiable spanwise structures. Bandyopadhyay (1991) has demonstrated via careful visualization studies that near reattachment these spanwise structures are not well identifiable and are more clearly three-dimensional. The flow is characterized, instead, by longitudinal vortex pairs whose spanwise spacing is significantly lower than that of the vortex pairs which appear in boundary layers. He found that these paired eddies disintegrate quite rapidly beyond reattachment and smaller-scale motions quickly develop; it is this process which leads to the sudden fall in the Reynolds stresses. An alternative but possibly complementary way of explaining the fall is provided by Chandrsuda & Bradshaw (1981), who found that the energy dissipation rate and the loss of energy (from the wall region) via velocity triple-product transport both remain high beyond reattachment.

In the present flows, the long-lived high transport rates are implied by the behaviour of the transport velocity defined by $V' = (\overline{vu^2}+\overline{v^3})/(\overline{u^2}+\overline{v^2})$ which, as CE showed, remains high in the outer part of the flow for a considerable downstream distance. Figure 19 shows an alternative way of considering the triple-product data; profiles of the 'diffusion function', $G_d = \frac{3}{4}(\overline{u^2v}+\overline{v^3})/[-\overline{uv}(-\overline{uv}_{max})^{1/2}]$, are plotted at three values of x' and for both cases. Since an entrainment velocity (V'/U_e) proportional to $-\overline{uv}_{max}/U_e^2$ (which is roughly true for standard thin shear flows) implies that $G_d \propto [(-\overline{uv}_{max})/U_e^2]^{0.5}$ the diffusion function shown in the figure has been normalized by this quantity (i.e. $G_d' = G_d/[(-\overline{uv}_{max})/U_e^2]^{0.5}$).

Near reattachment G_d' values are similar to those on the high-velocity side of a plane mixing layer (which happen also to be similar to standard boundary layer levels). As development proceeds, however, G_d' first rises significantly across the entire flow. This is a result of the rapid fall in (squared) stress levels and the relatively less rapid reduction in the triple products. By $x' = 20$, for example, the stresses (particularly $\overline{uv}$) are not much above their standard boundary layer levels (figure 10*a*) whereas the peak $\overline{v^3}$, although it has fallen substantially, still remains about six times larger than its standard value (figure 14). Further downstream G_d' falls again but even at $x' \approx 70$ the profile remains substantially above standard levels. In the inner half of the flow there is actually no noticeable reduction in G_d' levels between $x' = 20$ and $x' = 70$ and here the levels are very similar to those in the HB reference case. It is clear that the outer layer structures continue to play a dominant role all the way to the final measurement

https://doi.org/10.1017/S0022112098002420 Published online by Cambridge University Press

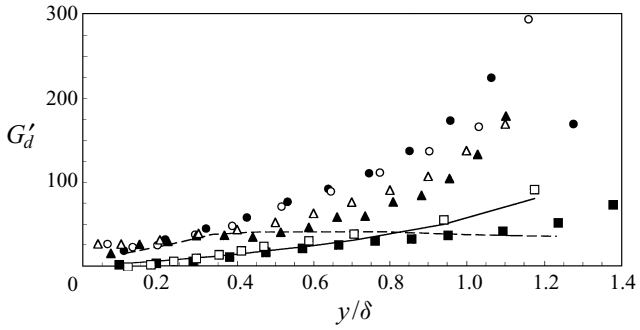


FIGURE 19. Diffusion function profiles. $G'_d = \frac{3}{4}(\overline{u^2v} + \overline{v^3})/[-\overline{uv}(-\overline{uv}_{max})]$. NFST: □, $x' = 2.83$; ○, 20.5; △, 71. FST: ■, $x' = 2.45$; ●, 17.7; ▲, 61.4; ——, standard boundary layer; ————, HB reference case ($u'/U_e = 0.0255$, $L_e/\delta = 0.77$).

station. As in the case studied by Alving & Fernholz (1996) the inner layer flow remains significantly different from normal. In their case the outer flow structures were essentially the remnants of the upstream boundary layer heavily distorted by the (relatively mild) separation/reattachment process. In the present case the reattachment flows are rather more energetic so it is perhaps not surprising that the outer flow structures are at least as long-lived. In this context we mention, finally, a result noted in our preliminary paper (CE). Intermittency data obtained indirectly by using the flatness factor data for the axial velocity component yielded cross-stream profiles very similar to those measured (directly) by Bandyopadhyay (1989). These were characterized by considerably lower values of the intermittency – all the way to the wall – than occur in a standard boundary layer and confirm the dominance of the outer large-scale structures. In the present cases, there was very little change in these abnormal profiles between the final two measurement stations ($x' = 40.7$ and 71 in the NFST case), again indicative of extremely slow metamorphosis of the large structures.

The measurements were generally not sufficiently extensive to obtain accurate estimates of all the (measurable) terms in the turbulent energy or shear stress balances. However, figure 20 shows the former at three stations in the NFST case; the advection term has been obtained by difference. At these locations the normal stress production and the axial diffusion terms were found to be insignificant. Strictly, therefore, the difference term must also include pressure diffusion, although this is normally reckoned to be small. At $x' = 2.83$ the balance (beyond the near-wall region, $y/\delta < 0.1$, say) looks very similar to that for (the outer two thirds of) a plane mixing layer. Energy is lost by turbulent transport from the inner half of the flow ($y/\delta < 0.4$ – the 'central' part of a plane mixing layer), where this loss reaches a peak almost as large as the dissipation peak, whilst further out transport is largely balanced by advection. At this location the data allowed reasonable estimation of the advection and the two sample values obtained are included in figure 20(*a*). They do not differ too greatly from the values obtained by difference, which gives some confidence that pressure diffusion is indeed small. The production term falls with downstream distance much more rapidly than the dissipation. At $x' = 10.3$ (figure 20*b*) production at $y/\delta = 0.5$ is a factor of 4.4 smaller than at $x' = 2.83$ whereas the corresponding factor for the dissipation term is only 2.3. This behaviour was also found by Chandrsuda & Bradshaw (1981) for the similar case of flow developing after a backward facing step and, along with the large loss by triple-product diffusion, explains why the stresses fall so rapidly.

The magnitude of the peak turbulent transport in the inner half of the flow (representing a loss of energy) falls much more rapidly than that of the outer flow peak

https://doi.org/10.1017/S0022112098002420 Published online by Cambridge University Press

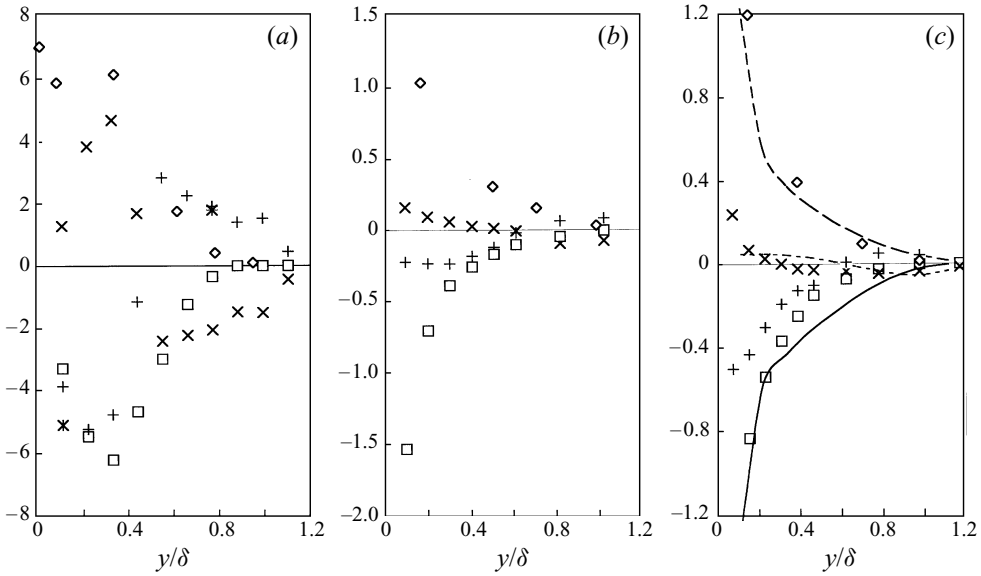


FIGURE 20. Turbulent kinetic energy balances, NFST. (*a*) $x' = 2.83$; (*b*) 40.7; (*c*) 71. $\times$, $\partial(\overline{q^2 v})/\partial y$ (diffusion); $\diamond$, ϵ (dissipation); $\square$, $uv(\partial U/\partial y)$ (production); $+$, $U\partial(q^2/2)/\partial y +$ other terms by difference. Quantities normalized using $(\delta/U_e^3)\,10^3$. In (*a*) $*$, measured advection. In (*c*) curves are standard boundary layer profiles of diffusion, dissipation and production.

(representing a gain in energy) and by $x' = 70$ its form remains measurably different from that for a standard boundary layer (figure 20*c*). Again, the form is similar to that found by Hancock in the HB reference case, with a maximum gain of about the same value and occurring around $y/\delta = 0.75$. However, the advection by difference is probably not sensible at $x' = 70$ and, assuming that pressure-diffusion is small, suggests some cumulative errors in determination of the other terms. Despite the uncertainties, however, the balances reinforce the picture deduced on the basis of the data presented earlier.

5. Numerical computations

Some calculations of these flows have been made using standard turbulence models. These were performed using a commercial CFD code (CFX 4); full details are given by Johnstone (1996) and are not presented here. Computations were undertaken for the NFST case using the standard k–ϵ model, a standard Reynolds stress model (including wall reflection functions) and the Launder–Sharma model. The latter allows calculations all the way to the wall, without the imposition of log-law conditions. Each model performed adequately when used for a standard zero-pressure-gradient boundary layer. For the developing flows, the computations started from initial (inlet) conditions set at the first measurement station ($x = 130$ mm), with all variables interpolated from cubic spline fits to the data. Grids typically had 100 cells in the x-direction and 50 in the y-direction, with very small expansion ratios (typically 1.02 in the axial direction). For the Launder–Sharma computations, the lateral grid had 100 cells to allow adequate coverage of the sub-layer region. The most striking feature of the results was the failure of either of the two more complex models to improve on the performance of the k–ϵ model. All three models failed to reproduce the eventual

https://doi.org/10.1017/S0022112098002420 Published online by Cambridge University Press

suppression of the turbulent stresses below standard values. Interestingly, the results obtained from the full Reynolds stress model were particularly poor, which may be related to the way in which the wall-reflection corrections are applied. Without these corrections, the near-wall behaviour of the stresses was, however, even more unrealistic.

Since the experiments indicated that the log law does not begin to re-appear until some way downstream of $x = 130$ mm, it might be argued that imposition of standard wall laws at that starting location (as necessary in the k–ϵ and RSM computations) would be bound to force significant errors. An additional set of calculations was done using inlet profiles measured at $x = 280$ mm (where there is a thin log law, figure 3*a*), but the general performance of the various models was not significantly improved. Curiously, the fact that the inlet boundary conditions did not correspond to a normal boundary layer (especially at $x = 130$ mm) seemed to affect the Launder–Sharma model rather more severely than the others. One might have expected the opposite, i.e. more severe failings might be anticipated from those models that require use of the wall law. However, it is known that the Launder–Sharma model generally underpredicts the turbulence levels in the inner layer of a normal boundary layer (due to its wall-damping function, see Patel, Rodi & Scheuerer 1984) so since the initial, near-wall turbulence levels in the present flows are very much higher than in standard boundary layers, it is perhaps not surprising that, for example, the initial wall-friction values are predicted to be much too high.

It is accepted that more sophisticated and specially tailored turbulence models would probably perform significantly better. But our intention in doing these calculations was simply to indicate that such models would, indeed, be necessary if accurate predictions of, say, the total surface drag (over the measurement region) were required. Whilst commercial CFD packages may often provide useful practical results for complex engineering flows, they should not generally be used as research tools for studying the details of such flows. The present (geometrically simple) cases of boundary layers developing after separated regions are simply too complex (fluid dynamically) for such an approach.

6. Conclusions

An experimental study of boundary layers developing subsequent to an initial separated region has been conducted. The general picture of an energetic outer layer decaying very slowly with downstream distance whilst, at the same time, preventing the inner layer from attaining its canonical form, is clear. By comparison with data obtained by other workers in different, but related flows, it seems that many of the features of the developing boundary layer are qualitatively independent of the precise nature of the separation and reattachment process. In addition, we have shown that changing the outer boundary condition (by adding stream turbulence) does not greatly alter the development process. Indeed, it is clear that the developing boundary layer has some characteristics similar to those that occur in boundary layers beneath stream turbulence. In particular, stress levels all across the layer eventually fall below those in standard boundary layers, at distances further downstream than probed previously and, even in the absence of stream turbulence, must require a spectacularly long downsteam fetch to recover to their expected levels. In the inner region, although the log law is eventually re-established (as found previously), the turbulence structure has not developed normally even by 70 boundary layer thicknesses downstream. Stream turbulence only marginally increases this rate of development but, of course, the flow must then eventually develop to one rather different from a standard boundary layer.

https://doi.org/10.1017/S0022112098002420 Published online by Cambridge University Press

This is all a result of the dominance of the energetic and relatively large-scale structures that exist around reattachment, which can only very slowly change their nature from 'mixing-layer-like' structures to those more common in canonical boundary layers. The results help to explain, among other things, the well-known fact that inappropriate tripping devices can produce turbulent boundary layers which never seem to reach normality. They also emphasize the general sensitivity of turbulent shear flows to initial conditions – a leading-edge 'bubble' will not yield a boundary layer of standard form – and they demonstrate that energetic large-scale motions can be extremely long-lived and relatively insensitive to less coherent perturbations.

The second author is grateful to the Royal Society of London, which supported a visit to Surrey during which the first stages of the experiment were undertaken. Comments by the authors' colleague, Dr Philip Hancock, on an earlier draft of this paper are gratefully acknowledged, as is the contribution of Mr Roderick Johnstone, who undertook the computations discussed in Section 5. The help of the Department's workshop staff was also invaluable; their contributions made the experiments possible. Finally, we thank the referees for a number of helpful suggestions.

REFERENCES

Adams, E. W. & Johnston, J. P. 1988 Flow structure in the near-wall zone of a turbulent separated flow. *AIAA J.* **26**, 932–939.

Alving, A. E. & Fernholz, H. H. 1996 Turbulence measurements around a mild separation bubble and downstream of reattachment. *J. Fluid Mech.* **322**, 297–328.

Alving, A. E., Smits, A. J. & Watmuff, J. H. 1990 Turbulent boundary layer relaxation from convex curvature. *J. Fluid Mech.* **211**, 529–566.

Bandyopadhyay, P. R. 1989 Instabilities and large structures in reattaching boundary layers. *AIAA J.* **29**, 1149–1155.

Bradshaw, P. 1971 *An Introduction to Turbulence and its Measurement*. Pergamon.

Bradshaw, P. & Wong, F. W. F. 1972 The reattachment and relaxation of a turbulence shear layer. *J. Fluid Mech.* **52**, 113–135.

Castro, I. P. 1979 Relaxing wakes behind surface-mounted obstacles in rough wall boundary layers. *J. Fluid Mech.* **93**, 631–659.

Castro, I. P. & Bradshaw, P. 1976 The turbulence structure of a highly curved mixing layer. *J. Fluid Mech.* **73**, 265–304.

Castro, I. P. & Epik, E. 1996 Boundary layer relaxation after a separated region. *Exptl Thermal Fluid Sci.* **13**, 338–348 (referred to herein as CE).

Castro, I. P. & Haque, A. 1987 The structure of a turbulent shear layer bounding a separation region. *J. Fluid Mech.* **179**, 439–468.

Castro, I. P. & Haque, A. 1988 The structure of a shear layer bounding a separated region. Part 2. Effects of free-stream turbulence. *J. Fluid Mech.* **192**, 577–595.

Chandrsuda, C. & Bradshaw, P. 1981 The turbulence structure of a reattaching mixing layer. *J. Fluid Mech.* **110**, 171–194.

Cherry, N. J., Hillier, R. & Latour, M. E. M. P. 1984 Unsteady measurements in a separating and reattaching flow. *J. Fluid Mech.* **144**, 13–46.

Compte-Bellot, G. & Corrsin, S. 1966 The use of a contraction to improve the isotropy of grid-generated turbulence. *J. Fluid Mech.* **25**, 657–682.

Counihan, J., Hunt, J. C. R. & Jackson, P. S. 1974 Wakes behind two-dimensional surface obstacles in turbulent boundary layers. *J. Fluid Mech.* **64**, 529–563.

Durbin, P. A. & Belcher, S. E. 1992 Scaling of adverse pressure gradient turbulent boundary layers. *J. Fluid Mech.* **238**, 699–722.

Dyban, E. P., Epik, E. Y. & Yushina, L. E. 1991 Influence of free stream turbulence on the development of a boundary layer after a separation region. *J. Appl. Thermosci.* **13**, 3–10.

https://doi.org/10.1017/S0022112098002420 Published online by Cambridge University Press

Erm, L. P. & Joubert, P. N. 1991 Low-Reynolds-number turbulent boundary layers. *J. Fluid Mech.* **230**, 1–44.

Fernholz, H. H. & Finley, P. J. 1996 The incompressible zero-pressure-gradient turbulent boundary layer: an assessment of the data. *Prog. Aerospace Sci.* **32**, 245–311.

Grant, H. L., Stewart, R. W. & Molliet, A. 1962 Turbulence spectra from a tidal channel. *J. Fluid Mech.* **12**, 241–268.

Hancock, P. E. 1980 The effect of free-stream turbulence on boundary layers. PhD Thesis, University of London.

Hancock, P. E. 1995 Reynolds number effects in separated flows. In *Advances in Turbulence V* (ed. R. Benzi), pp. 184–189, Kluwer.

Hancock, P. E. & Bradshaw, P. 1989 Turbulence structure of a boundary layer beneath a turbulent free stream. *J. Fluid Mech.* **205**, 45–76.

Hancock, P. E. & Castro, I. P. 1993 End effects in nominally two-dimensional separated flows. *Appl. Sci. Res.* **51**, 173–178.

Hillier, R. & Cherry, N. J. 1981 The effects of stream turbulence on separation bubbles. *J. Wind Engng Ind. Aero.* **8**, 49–58.

Johnson, A. E. & Hancock, P. E. 1991 The effect of extra strain-rates of streamline curvature and divergence on mixing layers. In *Turbulent Shear Flows 7* (ed. F. Durst *et al.*), pp. 253–267. Springer.

Johnstone, R. 1996 Finite-volume computation of boundary layer relaxation after a separated region. *Dept. Mech. Eng., University of Surrey Rep.* ME-FD/96.65.

Jovic, S. 1993 An Experimental Study on the Recovery of a Turbulent Boundary Layer Downstream of Reattachment. In *Engineering Turbulence Modelling and Experiment 2* (ed. W. Rodi & F. Martelli), pp. 509–517. Elsevier.

Jovic, S. & Browne, L. W. B. 1990 Turbulent heat transfer mechanism in a recovery region of a separated flow. In *Engineering Turbulence Modelling and Experiments* (ed. W. Rodi & E. N. Ganic), pp. 789–798. Elsevier.

Kim, J., Kline, S. J. & Johnston, J. P. 1980 Investigation of a reattaching turbulent shear layer. *Trans. ASME J. Fluids Engng* **102**, 302.

Kiya, M. & Sasaki, K. 1983 Structure of a turbulent separation bubble. *J. Fluid Mech.* **137**, 83–113.

Narasimha, R. & Prabhu, A. 1972 Equilibrium and relaxation in turbulent wakes. *J. Fluid Mech.* **54**, 1–17.

Patel, V. C. 1965 Calibration of the Preston tube and limitations on its use in pressure gradients. *J. Fluid Mech.* **23**, 185–208.

Patel, V. C., Rodi, W. & Scheuerer, G. 1984 Turbulence models for near-wall and low-Reynolds number flows. *AIAA J.* **23**, 1308–1319.

Perry, A. E., Lim, K. L. & Henbest, S. M. 1987 An experimental study of the turbulence structure in smooth- and rough-wall boundary layers. *J. Fluid Mech.* **177**, 437–466.

Phillips, W. R. C. 1994 On the logarithmic-law constants and the turbulent boundary layer at low Reynolds numbers. *Appl. Sci. Res.* **52**, 279–293.

Ruderich, R. & Fernholz, H. H. 1986 An experimental investigation of a turbulent shear flow with separation, reverse flow and reattachment. *J. Fluid Mech.* **163**, 283–322.

Smits, A. J. & Wood, D. H. 1985 The response of turbulent boundary layers to sudden perturbations. *Ann. Rev. Fluid Mech.* **17**, 321–358.

Smits, A. J., Young, S. T. B. & Bradshaw, P. 1979 The effects of short regions of high surface curvature on turbulent boundary layers. *J. Fluid Mech.* **94**, 209–242.

https://doi.org/10.1017/S0022112098002420 Published online by Cambridge University Press